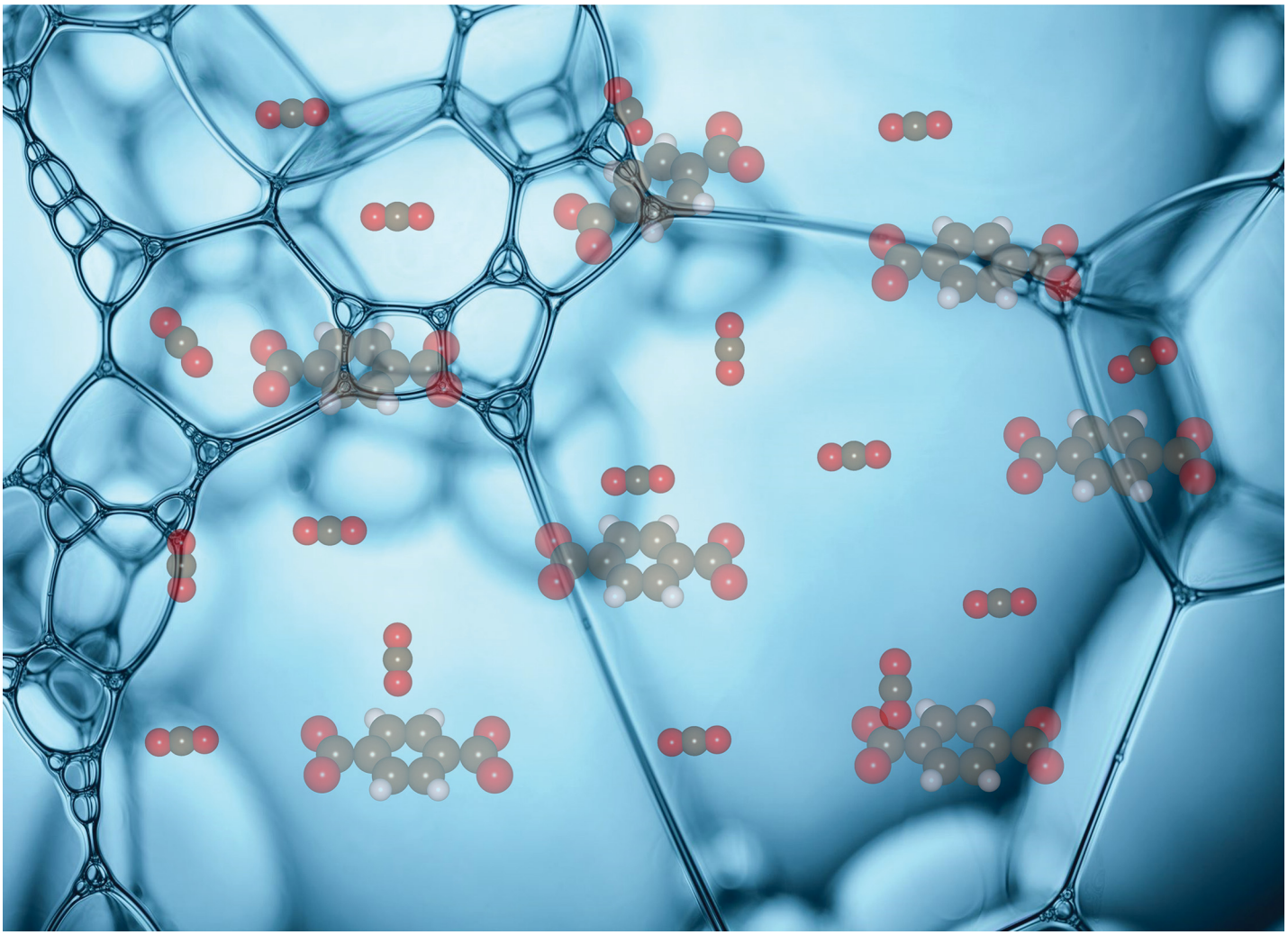

**Showcasing research from Dr Srimanta Pakhira's laboratory at the Indian Institute of Technology Indore (IIT Indore)**

Designing organic bridging linkers of metal–organic frameworks for enhanced carbon dioxide adsorption

This work gives an idea of the $CO_2$ adsorption at the center and side position of the organic bridging linkers of metal–organic frameworks (MOFs) that can be integrated into MOFs for enhanced $CO_2$ adsorption.

## As featured in:

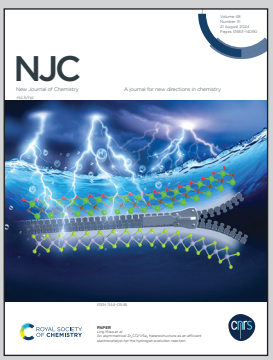


See Kahkasha Parveen and Srimanta Pakhira, *New J. Chem.*, 2024, **48**, 13700.

ROYAL SOCIETY OF CHEMISTRY

rsc.li/njc

Registered charity number: 207890

NJC

ROYAL SOCIETY OF CHEMISTRY

PAPER

View Article Online
View Journal | View Issue



Cite this: *New J. Chem.*, 2024, **48**, 13700

# Designing organic bridging linkers of metal–organic frameworks for enhanced carbon dioxide adsorption†

Kahkasha Parveen [a] and Srimanta Pakhira *[ab]

The global rate of anthropogenic carbon dioxide ($CO_2$) emission is rising, which urges the development of efficient carbon capture and storage (CCS) technologies. Among the various $CO_2$ capture methods, adsorption by metal–organic framework (MOF) linkers as excellent $CO_2$ adsorbents has attracted immense interest because of their important role in understanding the interaction mechanism for $CO_2$ adsorption. Here, we have investigated the adsorption of a $CO_2$ molecule at the center and side positions of eight MOF-linkers using molecular cluster models. The interaction between $CO_2$ and the linkers is assessed by computing the binding enthalpy ($\Delta H$) through the first principles-based density functional theory (DFT) with Grimme's dispersion corrections (*i.e.*, B3LYP-D3) and second-order Møller Plesset theory (MP2) methods. The results of our investigations revealed that the center and side positions of the FBDC, DFBDC-1, DFBDC-2, and TFBDC linkers, the side position of the DClBDC-2 linker, and the center position of the NDC linkers exhibit favorable physisorption behavior for $CO_2$ adsorption, with the values of $\Delta H$ ranging from −12.05 to −14.09 kJ mol$^{-1}$. After lithium (Li) decoration on the pure linkers, $CO_2$ adsorption at the center position of the BDC, FBDC, and DClBDC-1 linkers and the side position of the BDC, FBDC, DFBDC-1, and DFBDC-2 linkers reflects a strong physisorption behavior with the values of $\Delta H$ lying in the range of −34.64 to −35.30 kJ mol$^{-1}$ but remaining below the energy of a chemical bond (chemisorption), which is required for facile $CO_2$ release. To support our computed results, energy decomposition analysis (EDA) has been performed and the EDA study reveals that among all the energy components, the contribution of electrostatic and polarization energy components to the $\Delta H$ value is the most dominant. Frontier molecular orbital (FMO) analysis demonstrated the stability of the Li-decorated linkers. The results of our investigations will direct the development and synthesis of novel porous MOFs with enhanced $CO_2$ adsorption.

Received 14th March 2024,
Accepted 28th June 2024

DOI: 10.1039/d4nj01197j

rsc.li/njc



## 1. Introduction

Burning fossil fuels for power generation and transportation leads to the emission of many greenhouse gases into the environment causing pollution, climate change, and harmful impacts on human health. Carbon dioxide ($CO_2$) is believed to be one of the main greenhouse gases and has triggered serious global climate change.[1] Thus, to reduce the emission of $CO_2$ and minimize the impact of greenhouse gases on the environment, the development of feasible technologies for efficient $CO_2$ capture is highly required.[2] The captured $CO_2$ can be reused as a source of carbon and can be effectively converted into sustainable and value-added fuels such as methane, methanol, formaldehyde, *etc.*[3,4] Among the various techniques such as chemical absorption, adsorption, cryogenic and membrane separation, carbon capture and storage (CCS) by solid porous adsorbents has evolved as an innovative strategy that can be used to reduce the emission of $CO_2$.[5–7] Adsorption by porous materials presents the advantages of quick recovery, high adsorption capacity in humid environments, simple handling, and materials' stability.[8] However, the most challenging task at present is to develop efficient adsorbents with high adsorption capacity, thermal and chemical stability, fast kinetics, low cost and reversible $CO_2$

[a] *Theoretical Condensed Matter Physics & Advanced Computational Materials Science Laboratory, Department of Physics, Indian Institute of Technology Indore (IIT Indore), Simrol, Khandwa Road, Indore, Madhya Pradesh, 453552, India. E-mail: spakhira@iiti.ac.in, spakhirafsu@gmail.com*

[b] *Theoretical Condensed Matter Physics & Advanced Computational Materials Science Laboratory, Centre for Advanced Electronics (CAE), Indian Institute of Technology Indore, Simrol, Khandwa Road, Indore, Madhya Pradesh, 453552, India*

† Electronic supplementary information (ESI) available: Binding enthalpy of both the pristine and Li-decorated linkers at the center and side positions of the linkers, energies of the HOMO and LUMO for $CO_2$ adsorption at the side positions of all the linkers, all the coordinates of the equilibrium structure including linkers, and both the pure and Li-decorated linkers after $CO_2$ adsorption at the center and side positions. See DOI: https://doi.org/10.1039/d4nj01197j

 

uptake and release properties. A wide variety of adsorbents such as covalent organic frameworks (COFs),[9] metal–organic frameworks (MOFs),[10,11] and zeolites[12–15] have been employed for the storage, capture, and separation of $CO_2$, $H_2$, $CH_4$, and $N_2$ from a mixture of gases.

MOFs are a class of crystalline nanoporous materials that have been used for several applications such as gas storage and separation processes, catalysis, sensing, *etc.*[16–18] These materials are advantageous for the adsorption and separation of gases owing to their (1) physical, thermal, and chemical stabilities, which make them ideal for use as adsorbents under harsh conditions; (2) high surface areas and pore volumes, which help in the storage and capture of adsorbates; and (3) the outstanding tunability, which helps them to improve their adsorption performance through some modifications. As a class of MOFs, IRMOFs have the potential to be used as excellent adsorbents. The ability of the MOF materials to be synthesized using different bridging linkers/ligands and metal ions/clusters provides enormous flexibility in the design of these porous materials with tunable pore size, pore volume, and high surface area.[19,20] These properties have made MOF materials an attractive choice for the adsorption of gases in modern science and technology; however, only a few studies have been performed on $CO_2$ capture using a molecular cluster model. The first member of the MOF family (*i.e.*, IRMOF-1) was synthesized using $Zn_4O$ as a metal node and benzenedicarboxylate (BDC) as an organic linker and has been widely investigated for storage of $H_2$, $CO_2$, and $CH_4$.[21–23] The other members of the IRMOF family are formed by replacing either the benzene ring with larger aromatic rings or the C and H atoms of the rings with heteroatoms and functional groups respectively. It has been found that among the various IRMOFs-*n* ($n$ = 3, 6, 8, 11, 18) studied, the $CO_2$ adsorption capacity of IRMOF-1 is the highest and hence pristine IRMOF-1 acts as an excellent adsorbent for $CO_2$.[24] A study conducted by Liu *et al.* explained the adsorption mechanism of $CO_2$ on linkers of IRMOF-1 using a density functional theory (DFT) method. The authors studied eight different positions with three orientations of $CO_2$, suggesting that the side position with $CO_2$ parallel attack at the hydrogen side of the linker edge is the most favorable adsorption site.[23] Yang *et al.* studied the effect of organic linkers on the $CO_2$ adsorption capacity of MOF materials and revealed that MOFs with larger surface area and free volume have a high storage capacity of $CO_2$.[25] Moreover, Torrisi *et al.* analyzed the intermolecular interactions between $CO_2$ molecules and several functionalized aromatic molecules using the DFT method to guide the design of organic linkers that can form new materials with enhanced energy for $CO_2$ adsorption.[26,27] These studies suggest that interaction energy, positions, and orientations of the gas molecule, along with the organic linkers of the MOF materials, promote the understanding of the adsorption mechanism of $CO_2$ and design of novel MOFs with high uptake. However, due to the low reactivity (interaction energy) of the adsorbate or linker surface, the adsorption of $CO_2$ on the pristine MOF linkers belongs to the weak physical adsorption, limiting the practical application of MOFs as adsorbent materials. According to the findings of earlier research, altering the adsorbate surface through techniques like metal doping or decoration, chelation, functionalization, and ligand/linker modification boosts the chemical reactivity of the substrate and strengthens the interaction between the gas molecules and the linker-based materials.[28–35] Thus, the increased strength of interaction with the surface (linker) will help in understanding the interaction mechanism of $CO_2$ adsorption and the design of ideal adsorbate materials for gas storage applications. MOFs synthesized using benzenetricarboxylate (BTC) and benzenedicarboxylate (BDC) linkers are known for their high thermal and hydrolytic stability as well as intrinsic porosity and these two linkers (BDC and BTC) have shown enhanced binding strength with the frameworks, resulting in a significant amount of $CO_2$ adsorption. Aprea *et al.* reported the isosteric heat of $CO_2$ adsorption ($Q_{st}$) on a polymeric copper(II) benzene-1,3,5-tricarboxylate (Cu-BTC) MOF to be 25.9 kJ mol$^{-1}$.[36] Another experimental study conducted by Liu *et al.* reported that $CO_2$ adsorption on a series of functionalized MIL-47-X (where X = Cl, Br, $CH_3$, $CF_3$, OH, $OCH_3$) MOFs containing BDC as their constituent organic linker reached a maximum value of $Q_{st} \sim -24.99$ kJ mol$^{-1}$.[37] Besides increased strength of interaction, their high stability will likely establish MOFs as the next generation of materials for practical $CO_2$ capture. Using fluorinated ligands is an effective approach for creating a highly stable, rigid, and multidimensional framework with a highly crystalline phase.[38,39] The –F moiety attached either to the ligand or trapped within the pores helps to stabilize the MOFs and acts as a structure-directing agent that influences the final topology of MOFs.[40]

In this work, we have computationally designed eight MOF linkers *i.e.*, 1,4-benzene dicarboxylate (BDC), 3-fluoro-1,4-benzene dicarboxylate (FBDC), 3,6-difluoro-1,4-benzene dicarboxylate (DFBDC-1), 2,3-difluoro-1,4-benzene dicarboxylate (DFBDC-2), 2,3,5,6-tetrafluoro-1,4-benzene dicarboxylate (TFBDC), 3,6-dichloro-1,4-benzene dicarboxylate (DClBDC-1), 2,3-dichloro-1,4-benzene dicarboxylate (DClBDC-2), and 1,4-naphthalene dicarboxylate (NDC) using molecular cluster model systems. Our work aims to study the substitutional effect of halogen atoms (namely fluorine and chlorine) on the $CO_2$ adsorption mechanism at the center and side positions of the linkers and predict the strength of interaction between the fluorinated and chlorinated linkers and $CO_2$ molecules for the future design of hydrophobic MOFs. Although some studies have been conducted on $CO_2$ adsorption on fluorinated MOFs, the effect of the number and position of –F and –Cl atoms on the organic bridging linkers of MOFs using the molecular cluster model has not been reported previously. Here, we employed the first principles-based hybrid periodic DFT method with van der Waals (in short vdW) corrections (*i.e.*, Grimme's-D3 dispersion corrections) to calculate the equilibrium geometries of the complexes. The single point energy of the equilibrium structures of the systems considered here has been computed by both the DFT (B3LYP-D3) and second-order Moller Plesset theory (MP2) methods. The study of binding or relative enthalpy ($\Delta H$) shows the weak interaction of the $CO_2$ molecule with the pristine linkers, so the strategy of Li-decoration has been used to determine its effect on the $\Delta H$ value. We computationally found that among all the complexes, $CO_2$ adsorption at the center position of the Li-decorated BDC, FBDC, and DClBDC-1 linkers and the side position of the BDC, FBDC,

DFBDC-1, and DFBDC-2 linkers shows strong physisorption interaction, which is essentially required for facile $CO_2$ release. Further to explain the interaction mechanism and find the contribution of different energy components/terms to the $\Delta H$ value, Energy Decomposition Analysis (EDA) was performed, and both the electrostatic and polarization energy components were found to be the most dominant ones. Also, to check the stability of the complexes, Frontier Molecular Orbital (FMO) analysis was performed at the equilibrium structure of the complexes, which showed a strong interaction, and it was found that the complexes remained stable even after Li-decoration.

## 2. Methods and computational details

Various computational studies have been performed at different levels of theory to explain the interaction mechanism of gases with the IRMOF-1 framework.[23,41–43] Here, the mechanism of $CO_2$ adsorption on the linkers has been investigated by employing the first principles-based unrestricted hybrid density functional theory (UDFT) B3LYP method. The equilibrium structures, geometries, energies of the molecular orbital, and the contribution of different energy components to the relative enthalpy ($\Delta H$) of the complexes were obtained by employing the B3LYP DFT method with Grimme's 3rd order dispersion corrections implemented in the Gaussian16 suite code.[44] The strength of the interaction of the $CO_2$ molecule with the linkers was evaluated by computing the single point energy of the complexes at the equilibrium geometries performed by using the B3LYP DFT method. To incorporate the long-range weak vdW dispersion effects between the atoms of the complexes, Grimme's dispersion correction parameter (D3) has been added to the DFT approach (*i.e.*, B3LYP-D3), which is necessary for the weakly bound systems.[45–51] The hybrid B3LYP functional has been widely used for geometry optimization of systems containing metal atoms in their constitution, providing an accurate description and fair indication of the interaction energy.[52] We further calculated the $\Delta H$ at the second-order Moller Plesset (MP2) level of theory, which is a more accurate *ab initio* method. We took the relaxed structures obtained from the B3LYP-D3 method and calculated the single point energies at the MP2 level to obtain the $\Delta H$ value. In contrast to DFT-D methods, the MP2 method does not rely on empirical parameters. Although the MP2 method can accurately predict the weak vdW forces, this method suffers from the disadvantage of time consumption and its applicability to large systems. So, to reduce computational costs, DFT methods with Grimme's dispersion corrections have been used in most places instead of the high computational cost MP2 method. Moreover, the DFT-D method offers a good balance between accuracy and computational efforts. Further to describe the structures and properties of organic linkers as well as metals, it is important to choose an appropriate basis set; hence, the correlation consistent polarization valence triple-$\zeta$ quality Gaussian basis set (cc-pVTZ) has been used to perform all the calculations like getting the equilibrium geometries and defining the atomic orbitals of all the atoms in the linkers.[53] This basis set is advantageous over other basis sets as it contains a higher basis function for each atom and gives much better results with high accuracy in the calculations. Using the same methods and basis sets, frequency (*i.e.*, harmonic vibrational analysis) and thermodynamic calculations were performed to obtain the value of $\Delta H$ and confirm the stable geometry of the complexes. All the structures were optimized without any symmetrical constraints and the optimized minimum-energy structures were confirmed to be stationary points on the potential energy surface. The equilibrium structures of all the complexes were visualized by using the Chemcraft.[54] We used GaussView 6.1[55] for the pictorial representation of various adsorption sites, and this is a graphical interface implemented in Gaussian16.[44]

The calculation of relative or binding enthalpy ($\Delta H$) includes geometry optimizations of both the pristine/pure and Li-decorated linkers with one $CO_2$ molecule adsorbed onto the center and side positions. After obtaining the equilibrium structure, the values of $\Delta H$ were calculated using the same B3LYP-D3 and MP2 methods. To check the performance of both the methods, eqn (1) and (2) were used to calculate the values of $\Delta H$ for both the pure and Li-decorated systems, respectively.

$$\Delta H_{CO_2} = H_{(linker+CO_2)} - (H_{linker} + H_{CO_2}) \quad (1)$$

$$\Delta H_{CO_2} = H_{(linker+Li+CO_2)} - (H_{linker+Li} + H_{CO_2}) \quad (2)$$

where $H_{(linker+CO_2)}$ represents the enthalpy of the adsorbate/substrate system in an equilibrium state with the $CO_2$ molecule, $H_{linker}$ represents the enthalpy of the linker, $H_{(linker+Li+CO_2)}$ is the enthalpy of the linker after Li decoration/adding to $CO_2$, $H_{linker+Li}$ is the enthalpy of the Li decorated linker, and $H_{CO_2}$ is the enthalpy of the $CO_2$ molecule. The negative value of the $\Delta H$ indicates that the adsorption of $CO_2$ is exothermic while a higher negative value of $\Delta H$ corresponds to a stronger adsorption. Calculation of the $\Delta H$ value is an essential factor affecting the MOF's ability to bind $CO_2$ and other gas molecules. Adsorption of gases on the MOF adsorbent would greatly benefit from an enhancement in the $\Delta H$ value. The temperature and pressure were kept at 298.15 K and 1.0 atm, respectively, for all the calculations. To calculate the enthalpy ($H$) of the systems, the electronic ($E_{elec}$), vibrational ($H_{vib}$), and zero-point vibrational energies (ZPE) were considered, and the following equation is used here:

$$H = E_{elec} + ZPE + H_{vib} \quad (3)$$

Finally, we computed the $\Delta H$ value by taking the differences. The energy decomposition analysis (EDA) has been performed using the scheme proposed by Su and Li popularly known as the localized molecular orbital energy decomposition analysis (LMO-EDA) to identify the contribution of different energy components to the total interaction energy.[56] The equilibrium geometries obtained by the UB3LYP-D3/cc-pVTZ level of theory were further used to perform the LMO-EDA using the General Atomic and Molecular Electronic Structural System "GAMESS" suite code.[57] In the case of LMO-EDA, the total interaction energy ($\Delta E_{int}$ or $\Delta H_{bind}$) of a system contains the contribution from electrostatic ($\Delta E_{els}$), exchange ($\Delta E_{exc}$), repulsion ($\Delta E_{rep}$), polarization ($\Delta E_{pol}$), and dispersion ($\Delta E_{dis}$) energy components. The total interaction energy was calculated using the expression shown in eqn (4).

 

$$\Delta H_{bind} = \Delta E_{els} + \Delta E_{exc} + \Delta E_{rep} + \Delta E_{pol} + \Delta E_{dis} \quad (4)$$

Each term in the LMO-EDA has its own significance. The electrostatic interaction ($\Delta E_{els}$) is understandable in terms of Coulomb's law, which prevents the molecular orbitals from mixing. The exchange interaction ($\Delta E_{exc}$) is caused by electron exchange and molecular delocalization. When two non-bonded atoms come closer at a certain distance overlap of their orbitals results in repulsion between the electrons of the atoms, giving rise to repulsion energy ($\Delta E_{rep}$). The polarization energy change ($\Delta E_{pol}$) is produced by polarizing the wave function of each monomer in response to the electric field of the other monomer. In molecules, the oscillators are coupled when they are close to each other. Because of the coupled fluctuating dipoles, the dispersion interactions ($\Delta E_{dis}$) also known as electrostatic interactions have been taken into account in the present computation.

Also, frontier molecular orbital (FMO) analysis has been performed to find the stability of the complexes showing a strong value of $\Delta H$. The geometries obtained by the UB3LYP-D3/cc-pVTZ level of theory were used to calculate the energies of the highest occupied molecular orbital (HOMO) and lowest unoccupied molecular orbital (LUMO). The energy difference or energy gap ($E_g$) between the HOMO and LUMO was calculated by using eqn (5).

$$E_g = E_{LUMO} - E_{HOMO} \quad (5)$$

where $E_{HOMO}$ and $E_{LUMO}$ are the energies of the HOMO and LUMO respectively.

## 3. Molecular system design and adsorption sites

The linkers studied here contain the basic building unit of the first synthesized MOF-5 (or IRMOF-1) material *i.e.*, the 1,4-benzene dicarboxylate (in short BDC) ligand or linker with halogen group elements attached to different positions of the BDC linker. These linkers contain hydrogen (H), carbon (C), oxygen (O), fluorine (F), and chlorine (Cl) atoms as their constituent atoms. BDC, commonly known as 1,4-benzene dicarboxylate, is basically a benzene ring with a carboxyl group attached at the para positions of the ring. FBDC is 3-fluoro 1,4-benzene dicarboxylate, where one fluorine is attached at the meta position of the BDC linker. DFBDC-1 and DFBDC-2 are difluoro-1,4-benzene dicarboxylates with two fluorine atoms attached to different positions of the BDC linker. In the case of DFBDC-1, one fluorine atom is attached at the meta position and the other is at the ortho position (*i.e.*, 3,6-difluoro-1,4-benzene dicarboxylate), whereas in the case of DFBDC-2, one fluorine is attached at the ortho while the other is at the meta position of the BDC ring (*i.e.*, 2,3-difluoro-1,4-benzene dicarboxylate). TFBDC is the 2,3,5,6-tetrafluoro-1,4-benzene dicarboxylate ligand, which is formed by attaching four fluorine atoms at both the ortho and meta positions. DClBDC-1 and DClBDC-2 are dichloro-1,4-benzene dicarboxylates with two chlorine atoms attached to different positions of the BDC linker. In the case of DClBDC-1, one chlorine is attached at the meta position, while the other is at the ortho position (*i.e.*, 3,6-dichloro 1,4-benzene dicarboxylate), whereas in the case of

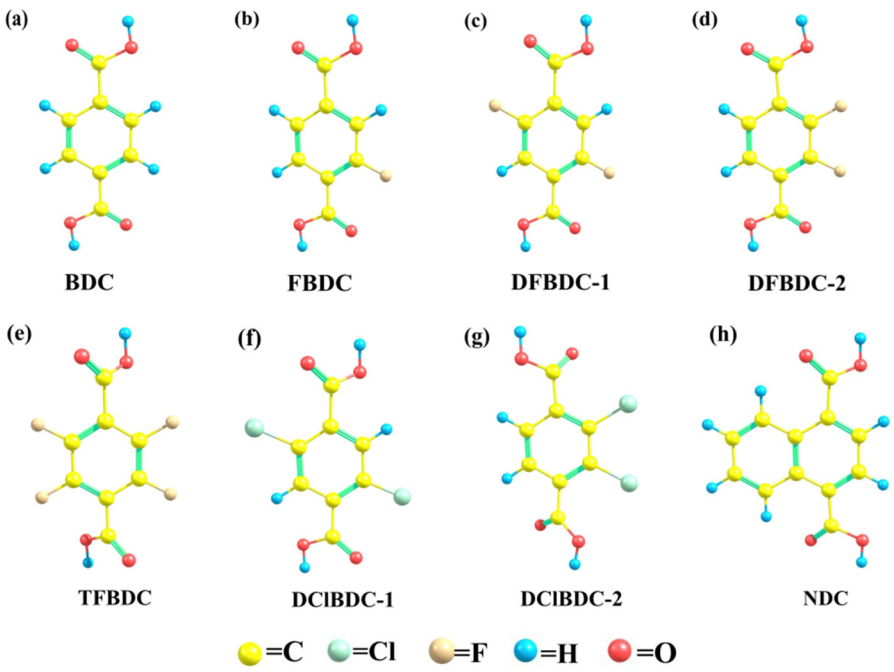


Fig. 1 The equilibrium structures of pure MOF linkers: (a) 1,4-benzene dicarboxylate (BDC), (b) 3-fluoro-1,4-benzene dicarboxylate (FBDC), (c) 3,6-difluoro-1,4-benzene dicarboxylate (DFBDC-1), (d) 2,3-difluoro-1,4-benzene dicarboxylate (DFBDC-2), (e) 2,3,5,6-tetrafluoro-1,4-benzene dicarboxylate (TFBDC), (f) 3,6-dichloro-1,4-benzene dicarboxylate (DClBDC-1), (g) 2,3-dichloro-1,4-benzene dicarboxylate (DClBDC-2), and (h) 1,4-naphthalene dicarboxylate (NDC).

DClBDC-2, one chlorine is attached at the ortho position, while the other is at the meta position (*i.e.*, 2,3-dichloro 1,4-benzene dicarboxylate) of the BDC ring. NDC is 1,4-naphthalene dicarboxylate, which is formed by a fused pair of benzene rings with carboxylate groups attached to the para positions. All the linkers considered in this work are depicted in Fig. 1.

In MOFs, the –COOH group is thought to be an excellent subsitute to ligand modification for $CO_2$ adsorption. Two types of interactions are attributed to the two distinct parts of the –COOH group. The hydroxyl uses the acidic proton to function as a Lewis acid, and the carbonyl group functions as a Lewis base. In the present work, the COOH groups attached to the linkers act as an excellent substitute for ligand modification for $CO_2$ adsorption. The high density of surface (–COOH) groups enhances the physisorption behavior with the increase in the value of binding energy. This effect is attributed to the lone pair donation of the oxygen in the group and carbon in the $CO_2$ and by hydrogen bond interactions of the acidic protons and the oxygen of $CO_2$.[58] Moreover, the COOH group attached to the linker tends to gain electrons from their neighboring carbon atoms, resulting in increased bonding interactions with the $CO_2$ molecule. The presence of oxygen-containing functionalities such as COOH increases the negative charge of the surface and hence changes the electronegativity of the surface. It also enhances the porosity of the surface, which leads to an increase in $CO_2$ adsorption capacity with the quadrupole moment. Furthermore, the introduction of polar functional groups such as –F, –Br, –Cl, –OH, –OOH, $-NO_2$, and $-SO_3$ in the organic linkers of MOFs can enhance $CO_2$ capacity, which is the result of interactions between the dipole of the polar functional group and the quadrupole moment of $CO_2$.[59] MOFs functionalized with –F and –Cl are effective approaches to introduce strong $CO_2$ adsorption sites on MOFs that can increase the binding affinity between the sorbents and $CO_2$. The F atoms are characterized by their high electronegativity and low polarizability, resulting in a highly polar C–F bond with a significant negative charge on the F atom as well as the hydrophobic nature of this bond. In other words, the high electronegativity and significant negative charge density of the F atom make it an ideal adsorption site within the MOF cavities. Consequently, fluorinated organic ligands are used in MOFs to enhance gas framework interaction due to the high porosity of the C–F bond and to increase water stability and hydrophobicity by incorporating F atoms into the pores.[60] While the F atom is the most commonly used halogen in the functionalized MOFs, Cl atoms are occasionally used as alternatives in the side chains of MOF aromatic skeletons to improve gas adsorption performance. Such functionalized MOFs usually display high $CO_2$ uptake capacity and high selectivity, even at very low concentrations.

To understand the adsorption mechanism in a porous material, it requires the knowledge of the adsorption sites of the adsorbate, so we chose the center and side positions of the linkers as the adsorption sites. We determined the equilibrium structures of other adsorption sites; unfortunately, the structures were not thermodynamically stable as they contain the imaginary frequency with the positive value of the relative enthalpy ($\Delta H$). For each system, the $CO_2$ molecule was placed perpendicularly to the center and side position of the pure and Li-decorated linkers. Fig. 2 depicts the orientation of the $CO_2$ molecule for its adsorption at the center and side positions of the BDC linker.

## 4. Results and discussion

### 4.1. Binding enthalpy

The change in enthalpy ($\Delta H$) is one of the deciding parameters in determining the stability of any hypothetical compound or complex system. A negative value of $\Delta H$ suggests that the structure is thermodynamically stable and can be synthesized experimentally. Here, the adsorption of $CO_2$ at the center and side positions of both the pristine and Li-decorated linkers has been investigated. The two different adsorption sites of $CO_2$ on the linkers can be understood by examining the bonding nature of $CO_2$ with the linkers.

At first, the adsorption of $CO_2$ on all the pristine linkers was studied and the strength of their interactions was investigated using eqn (1). The $CO_2$ molecule moved away from its original center and side positions after geometry optimization. The equilibrium geometries of the complexes are shown in Fig. 3, and the Cartesian coordinates of their equilibrium structures are provided in the ESI.† In this case, the value of $\Delta H$ lies in the range of $-8.07$ to $-14.09$ kJ mol$^{-1}$, computed by the B3LYP-D3 method, while the value lies between $-6.76$ and $-13.98$ kJ mol$^{-1}$ obtained by the MP2 method. It should be noted here that both the B3LYP-D3 and MP2 methods provide similar values of the $\Delta H$ within the range of DFT error. The computed values of $\Delta H$ are negative, which also indicates the stability and exothermic nature of the adsorption

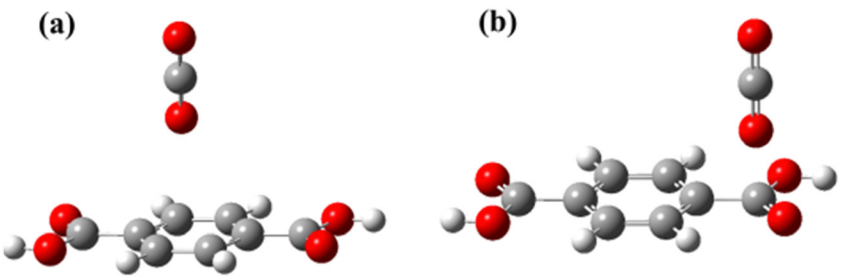


Fig. 2 The adsorption of the $CO_2$ molecule at the (a) center, and (b) side position of the BDC linker.

 

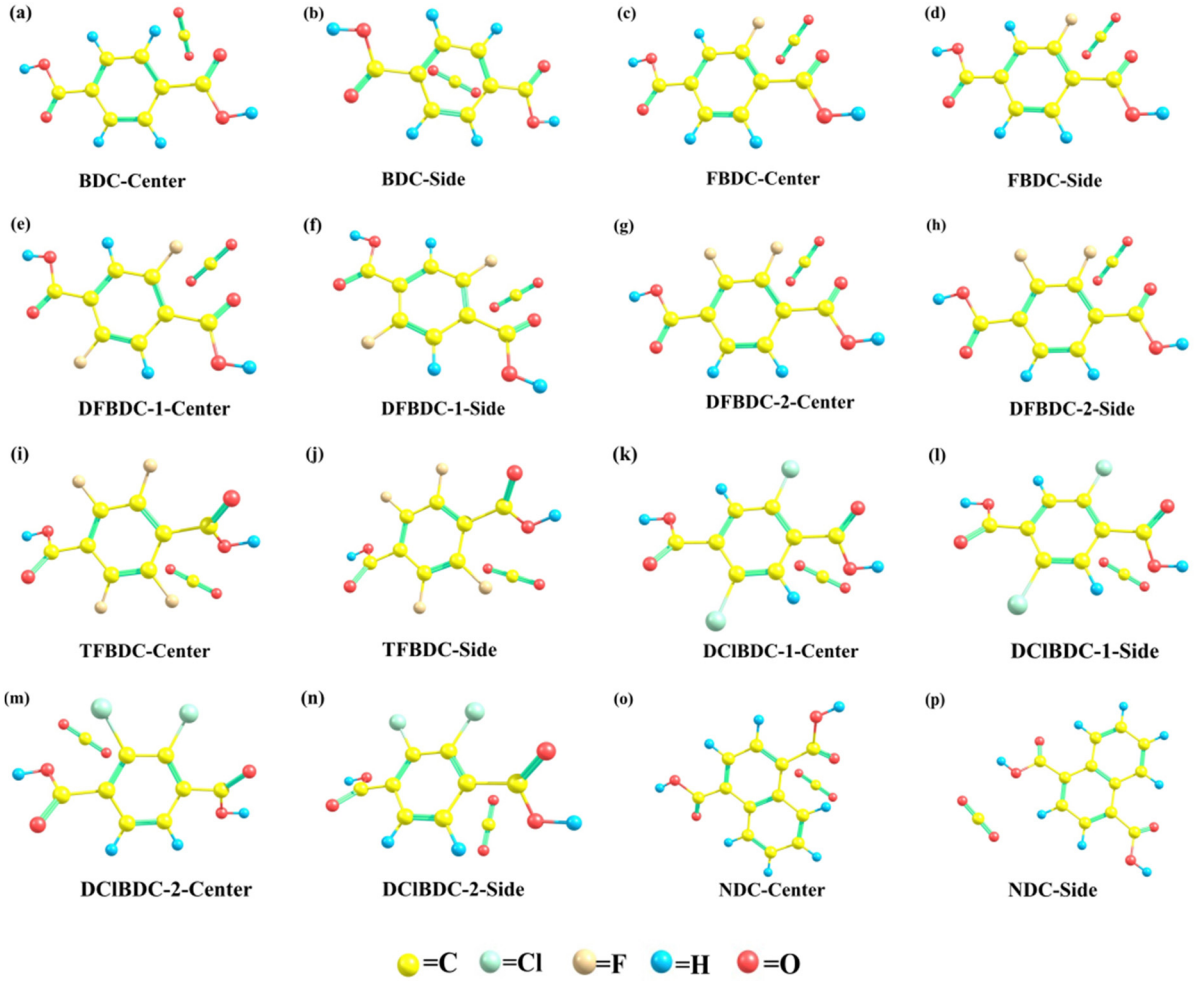


Fig. 3 Equilibrium structures of both the pristine linkers and the adsorbed $CO_2$ at the center and side positions of the linkers: (a) BDC - center, (b) BDC - side, (c) FBDC - center, (d) FBDC - side, (e) DFBDC-1 - center, (f) DFBDC-1 - side, (g) DFBDC-2 - center, (h) DFBDC-2 - side, (i) TFBDC - center, (j) TFBDC - side, (k) DClBDC-1 - center, (l) DClBDC-2 - side, (m) DClBDC-2 - center, (n) DClBDC-2 - side, (o) NDC - center, and (p) NDC - side.

processes. These values of $\Delta H$ indicate that $CO_2$ weakly interacts with the pristine linkers *via* vdW forces where the π electrons of the benzene ring constituting the linkers attract the positively charged carbon atom of $CO_2$. Moreover, from these calculations, we found the favorable adsorption sites of the $CO_2$ molecule. It is observed that $CO_2$ adsorption at the center and side positions of the FBDC, DFBDC-1, DFBDC-2, TFBDC linkers, the side position of the DClBDC-2 linker, and the center position of the NDC linkers shows favorable physisorption behavior with the value of $\Delta H$ in the range of $-12.05$ kJ mol$^{-1}$ to $-14.09$ kJ mol$^{-1}$. The highest binding configuration is observed for the NDC linker with one of the O atoms of $CO_2$ pointing towards the center of the six-membered ring, and this structure has the $\Delta H$ values of $-14.09$ and $-13.98$ kJ mol$^{-1}$ computed by the B3LYP-D3 and MP2 methods, respectively. This low negative value of $\Delta H$ indicates the large amount of $CO_2$ adsorption, and this is due to the increased surface area of the NDC linker, as it contains one extra benzene ring as compared to the other linkers. In other words, the double hydrocarbon ring of the NDC linker is expected to increase the pore and surface area of the NDC linker creating large space available for $CO_2$ adsorption near the center position, and as a result, there is an increment in $CO_2$ adsorption of the NDC linker. It is interesting to observe that the $CO_2$ adsorption at the side position of the NDC linker has the $\Delta H$ values of $-9.39$ kJ mol$^{-1}$ and $-6.76$ kJ mol$^{-1}$ computed by the B3LYP-D3 and MP2 methods respectively. This difference in the $\Delta H$ value at the center and side positions of the NDC linker is due to the surface area available for $CO_2$ adsorption and different kinds of interactions. In contrast, the side position of the NDC linker has less available area for the interaction of $CO_2$ with the linker and hence the values of relative enthalpy have increased as compared to the value at the center position. Additionally, it was found that fluorine and chlorine attached at the ortho and meta positions of the BDC linker significantly influence the value of $\Delta H$. In the case of fluorine atoms attached at the ortho and meta positions of the BDC linker, the value of $\Delta H$ increases (or $CO_2$ adsorption capacity decreases) with the number of fluorine atoms. The increase in the number of fluorine atoms reduces the surface area and pore volume of the linker along with a minor decrement in the $CO_2$ adsorption.[61] The same is observed for the FBDC,

DFBDC-1, DFBDC-2, and TFBDC linkers, where the value of $\Delta H$ increases with the number of fluorine atoms. This increased value of $\Delta H$ is consistent with the fluorinated triazine framework, where $CO_2$ uptake capacity decreased upon increasing the fluorine content, mainly due to the high molecular weight of the fluorine atom.[62] It is also observed that the value of $\Delta H$ increases with the attached chlorine atoms at the ortho and meta positions of the BDC linker forming DClBDC-1 and DClBDC-2 and as a result, it decreases the $CO_2$ adsorption capacity. Thus, we can say that $CO_2$ adsorption at the center and side positions of both the DFBDC-1 and DFBDC-2 linkers is more favorable than that on DClBDC-1 and DClBDC-2 linkers. This behavior of $CO_2$ adsorption is due to the electron-withdrawing properties of the halogen group elements, where destabilization of the complexes increases with the number of halogen groups. Moreover, the addition of fluorine (F) atoms tends to attract more electron/charge density from the $CO_2$ molecule *via* dispersive or van der Waals (vdW) forces, while the addition of chlorine destabilizes the π quadrupole interaction by withdrawing the charge of the π-aromatic system, resulting in the adsorption of fewer $CO_2$ molecules.

It is observed that the $CO_2$ adsorption at both the center and side positions of the FBDC, DFBDC-1, DFBDC-2, TFBDC linkers, the side position of the DClBDC-2 linker and the center position of the NDC linkers shows favorable physisorption behavior, while both the center and side positions of the BDC and DClBDC-1 linkers and the side position of the NDC linker do not show favorable physisorption. This behavior of the linkers is attributed to the amount of charge transfer that takes place between the linker and the $CO_2$ molecule. Transfer of charge/electrons plays an important role in determining the interaction of the adsorbate with the substrate. So, to explain the adsorption process, the charge transfer ($C_T$) between the linkers and $CO_2$ molecule has been calculated through Mulliken Population Analysis (MPA), and the calculated values of $C_T$ are provided in Table 1. The positive value of $C_T$ denotes the transfer of electrons from the linker to the $CO_2$ molecule, while the negative value denotes the electron transfer from the $CO_2$ molecule to the linker.[63] The values of binding enthalpy ($\Delta H$) and charge transfer ($C_T$) have a strong relation. The values of $C_T$ during $CO_2$ adsorption at both the center and side positions of the FBDC, DFBDC-1, DFBDC-2, and TFBDC linkers are $-0.016e$, $-0.015e$, $-0.014e$, and $-0.010e$, respectively, corresponding to the values of $\Delta H$ lying in the range of $-13.34$ kJ mol$^{-1}$ to $-12.05$ kJ mol$^{-1}$, and thus, they show favorable physisorption nature. $CO_2$ adsorption at the center and side positions of DClBDC-2 depends on the position of the chlorine atoms attached to the primary BDC linker. The center position shows a value of $\Delta H$ of about $-9.95$ kJ mol$^{-1}$ and a $C_T$ value of $-0.009e$, while the side position has a value of $-12.38$ kJ mol$^{-1}$ with a $C_T$ value of $-0.005e$. The weak $CO_2$ adsorption at both the center and side positions of the BDC and DClBDC-1 linkers and the side position of the NDC linker is attributed to the low $C_T$ value. The values of $C_T$ during the $CO_2$ adsorption at the side positions of both BDC and NDC are $0.004e$ and $0.008e$ respectively, indicating the transfer of charge from the linker to the $CO_2$ molecule and therefore this result suggests that the nature of the adsorption is mainly electrostatic interactions.

Table 1 The charge transfer ($C_T$) of the $CO_2$ molecule at the center and side positions of the pure and Li-decorated linkers

| Linkers | Position | $C_T$ ($e$) (Pure) | $C_T$ ($e$) (Li-decorated) |
|---|---|---|---|
| BDC | Center | −0.004 | 0.153 |
| | Side | 0.004 | 0.153 |
| FBDC | Center | −0.016 | 0.156 |
| | Side | −0.016 | 0.156 |
| DFBDC-1 | Center | −0.015 | −0.016 |
| | Side | −0.015 | 0.158 |
| DFBDC-2 | Center | −0.014 | −0.014 |
| | Side | −0.014 | 0.158 |
| TFBDC | Center | −0.010 | −0.015 |
| | Side | −0.010 | −0.015 |
| DClBDC-1 | Center | −0.007 | 0.159 |
| | Side | −0.007 | −0.013 |
| DClBDC-2 | Center | −0.009 | −0.014 |
| | Side | −0.005 | −0.009 |
| NDC | Center | −0.009 | −0.011 |
| | Side | 0.008 | −0.011 |

Next, we performed Li-decoration on the pristine linkers to determine their effect on the binding strength ($\Delta H$) of the $CO_2$ molecule. Due to the strong affinity of positively charged metal ions to the adsorbing gases, this strategy has been widely implemented for hydrogen storage.[34,64–67] Moreover, the choice of metal ions and their coordination environment plays a crucial role in the performance of MOFs for $CO_2$ adsorption. The introduction of a very low coordination number of a metal ion (CN = 2) in the simulation can be a useful strategy. This approach can induce interactions that may not be possible in the crystal structure of a MOF with a higher coordination number. The low coordination number of Li metal ions can lead to the creation of unsaturated or open metal sites. The presence of open metal sites corresponds to high $CO_2$ uptake, which is due to strong $CO_2$–metal interactions.[68] In other words, owing to the greater quadrupole moment and polarizability of the $CO_2$ molecule, these open metal cation sites serve as charge-dense binding sites, resulting in strong adsorption of $CO_2$ molecules. The adsorption of Li atoms on all the linkers forming Li-decorated complexes was studied by fully optimizing the structures, with Li atoms originally positioned near the O atoms of the COOH group attached to the six-atom carbon ring ($C_6H_4$ units). After geometry optimization, the lithium atom preferred to be in a position between the two neighboring oxygen atoms. The Li atoms decorated on each side of the linkers carry an average charge value of approximately $+0.2e$/Li atom to $+0.3e$/Li atom, suggesting the transfer of charges from the Li atoms to the linkers. To further investigate $CO_2$ capture, we optimized the structures with $CO_2$ positioned at both the center and side positions as was performed for the pristine linkers. The strong interaction of $CO_2$ with the linkers resulted in higher enthalpy of adsorption, which can be attributed to the large quadrupole moment of $CO_2$ as well as the presence of coordinatively unsaturated metal (Li) sites. Moreover, the structures were a little distorted after geometry optimization, which is attributed to the transfer of charges from the Li atoms to the linkers. The equilibrium geometries of the complexes are shown in Fig. 4 and

 

the Cartesian coordinates of the optimized structures are provided in the ESI.†

Based on the computed results of $CO_2$ adsorption on the Li-decorated linkers, it is observed that the value of $\Delta H$ at both the center and side positions of the BDC and FBDC linkers has been increased significantly. The side position of the DFBDC-1 and DFBDC-2 linkers and the center position of the DClBDC-1 linker are observed to show a drastic change in the $\Delta H$ value after Li-decoration. We find a reasonable quantitative agreement between our data calculated by both the methods and the experimentally synthesized $M_2$(dobdc) MOF systems.[69,70] This increment in $\Delta H$ is due to the large amount of charge transfer between the complexes. The center and side positions of the BDC and FBDC linkers have the $C_T$ values of 0.153*e* and 0.156*e* respectively, as provided in Table 1. Also, the values of $C_T$ at the side positions of DFBDC-1 and DFBDC-2 are 0.158*e*, while the center position of DClBDC-1 has a $C_T$ value of 0.159*e*. This positive value of $C_T$ indicates the charge transfer from the linker to the $CO_2$ molecule, indicating their high $CO_2$ adsorption at the center position and the possibility of their implementation as future porous MOF materials. The $CO_2$ adsorption at the center positions of DFBDC-1 and DFBDC-2 linkers and the side position of the DClBDC-1 linker exhibits $\Delta H$ values of $-16.85$ kJ mol$^{-1}$, $-11.25$ kJ mol$^{-1}$, and $-16.85$ kJ mol$^{-1}$. These values are attributed to the $C_T$ values of $-0.016e$, $-0.014e$, and $-0.013e$ respectively. It is further observed that the value of $\Delta H$ for the Li-decorated linkers with fluorine and chlorine attached at the ortho and meta positions does not follow the same trend as is observed in the case of pristine linkers. $CO_2$ adsorption at the center and side positions of both the TFBDC and DClBDC-2 linkers, the center position of the DFBDC-1 and DFBDC-2 linkers, and the side position of DClBDC-1 shows reversible physisorption. This behavior is evident from the calculated values of $\Delta H$, which are below the higher limit of physisorption. It is further noticed that the $CO_2$ adsorption at the center and side positions of the FBDC linker shows an approximate value of $\Delta H$ exceeding the higher limit of physisorption (*i.e.*, 20 kJ mol$^{-1}$), while still lying below the lower range of chemisorption (*i.e.*, 50 kJ mol$^{-1}$). The same behavior of $CO_2$ interaction is observed for the side position of the DFBDC-1 and DFBDC-2 linkers and the center position of the DClBDC-1 linker. These $\Delta H$ values indicate a strong physisorption behavior, and thus, the process of adsorption and desorption is reversible at room temperature. The values of $\Delta H$ during $CO_2$ adsorption at the center and side positions of the linkers computed by both the B3LYP-D3 and MP2 methods are shown in Fig. 5 and 6, respectively, and the calculated values of $\Delta H$ for both the pristine and Li-decorated linkers are provided in Tables S1 and S2 of the ESI.† Moreover, it is observed that the decoration of Li atoms on the NDC linker does not influence the $\Delta H$ value much, which was observed for the other Li-decorated linkers, despite its large surface area. Thus, we can say that the contribution of Li-atoms to the $CO_2$ adsorption of the NDC linker is not as significant as is observed for the other Li-decorated linkers

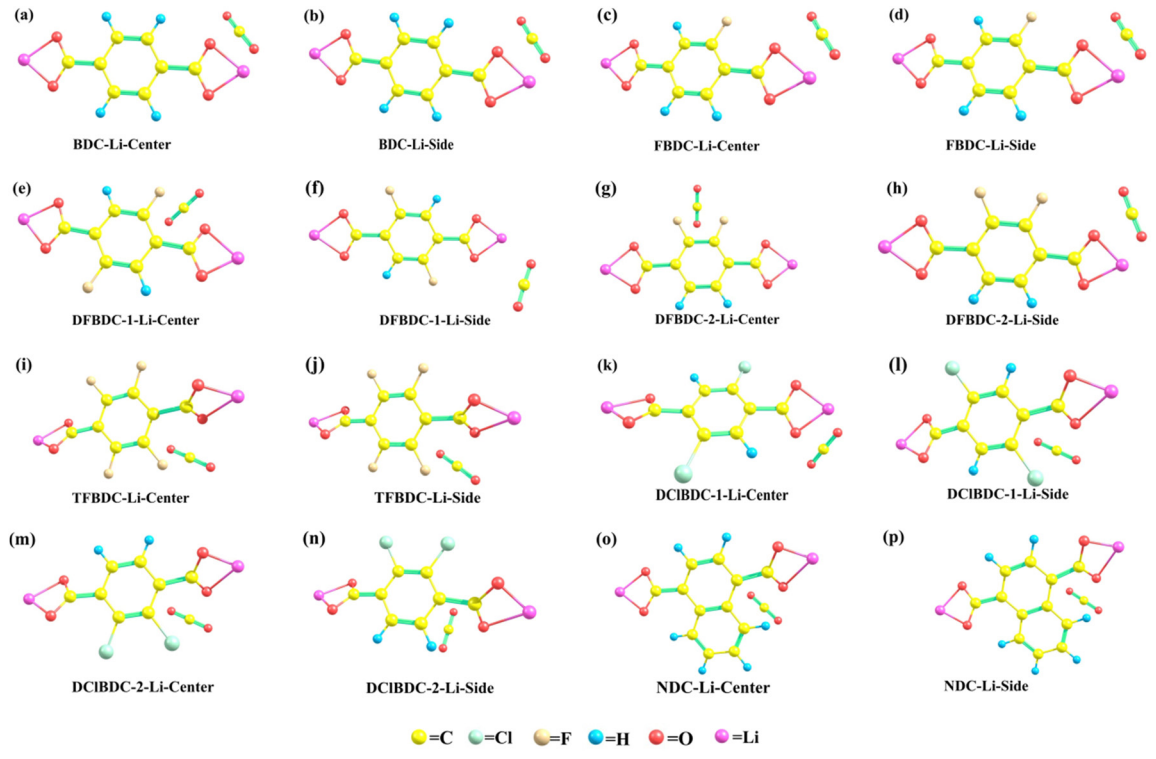


Fig. 4 Optimized structures of the Li-decorated linkers and the adsorbed $CO_2$ at the center and side positions: (a) BDC-Li - center, (b) BDC-Li - side, (c) FBDC-Li - center, (d) FBDC-Li - side, (e) DFBDC-1-Li - center, (f) DFBDC-1-Li - side, (g) DFBDC-2-Li - center, (h) DFBDC-2-Li - side, (i) TFBDC-Li - center, (j) TFBDC-Li - side, (k) DClBDC-1-Li - center, (l) DClBDC-2-Li - side, (m) DClBDC-2-Li - center, (n) DClBDC-2-Li - side, (o) NDC-Li - center, and (p) NDC-Li - side.

showing favorable physisorption behavior. $CO_2$ adsorption at the center and side positions of the NDC linker has an equal amount of $C_T$ value. Also, the hybridization between the $CO_2$ molecule and the Li atoms is weak, which indicates that the interaction between the $CO_2$ molecule and the linker originates mainly from the electrostatic ion and quadrupole moment of the $CO_2$ molecule and a major part of the electron/charge density comes from the atoms constituting the pristine NDC linker, which is depicted under the NBO analysis section. The results obtained from the harmonic vibrational analysis of $CO_2$ adsorption on both the pristine and Li-decorated linkers show no imaginary frequency, indicating that all these structures correspond to the local minima on the potential energy surface, which are thermodynamically stable in nature. In other words, the absence of imaginary frequencies assures the local minima of the equilibrium geometries of the complexes on the potential energy surface. These negative values of $\Delta H$ indicate that the practical formation of porous materials using these linkers can be possible, and the present calculations suggest the synthesis of the MOFs with application in $CO_2$ capture experimentally. These linkers show strong affinity for the $CO_2$ molecule and hence can be used as efficient adsorbents for the future design of ideal porous materials, especially MOFs.

Based on the above discussion, it can be stated here that the $CO_2$ adsorption on the Li-decorated linkers shows strong physisorption behavior with the $\Delta H$ lying below the chemisorption range, and these linkers are excellent candidates for $CO_2$ adsorption. This significant increase in the binding strength can probably be attributed to the combination of the high electrostatic interaction of $CO_2$ with the Li-atoms and the polar fluorinated and chlorinated pore surface of the framework. The main purpose of this study is to suggest the synthesis and predict the properties of these linkers towards $CO_2$ capture, and none of the linkers studied here have been integrated into a MOF or synthesized experimentally. However, the calculated vibrational frequencies and binding enthalpies predict that the systems are thermodynamically stable. Both the frequency analysis and binding enthalpy have been shown to demonstrate a material's stability and *a posteriori* synthesis in previous works.[28,29] The Li-decoration gives an accurate representation of the effect of metal units on the organic linkers. Indeed, increasing the length of the organic linkers results in a higher surface area of MOFs with enhanced gas adsorption. Nevertheless, extending the organic linker often compromises the stability of the MOFs. When $CO_2$ molecules are desorbed, there is a tendency for the system to partially or entirely collapse, resulting in reduced porosity or even non-porous frameworks. Consequently, creating a more stable MOF framework with increased porosity remains a significant challenge. Moreover, it is important to acknowledge that the $CO_2$ adsorption in practical applications always takes place in the presence of water. Thus, hydrophobic frameworks are ideal for capturing $CO_2$ in humid environments. Despite water's large dipole moment causing it to interact more strongly with most frameworks than $CO_2$, the hydrophobic nature of some MOFs enables them to minimize competitive water adsorption. In this regard, selecting MOFs known for their high chemical and thermal stability will be crucial in the future. Thus, we expect that these linkers can be integrated into MOFs, which will have potential application in $CO_2$ capture, and the present work will guide the researchers to synthesize these materials, which may be readily fabricated experimentally in the future for industrial applications.

Pore volume is another crucial factor in evaluating the porosity of MOFs. Consequently, designing MOFs with high porosity and creating effective methods to preserve and utilize their pore space have been a key focus in MOF research. Organic linkers are crucial in forming pore structures and by

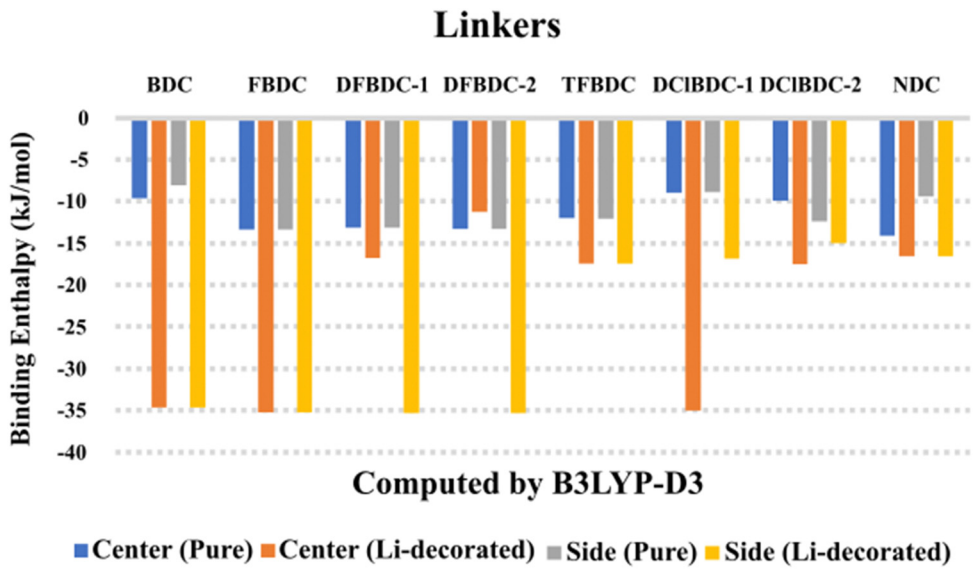


Fig. 5 The binding enthalpy ($\Delta H$) value of the adsorbed $CO_2$ molecule at the center and side positions of both the pure and Li-decorated linkers computed by the B3LYP-D3 DFT method.

 

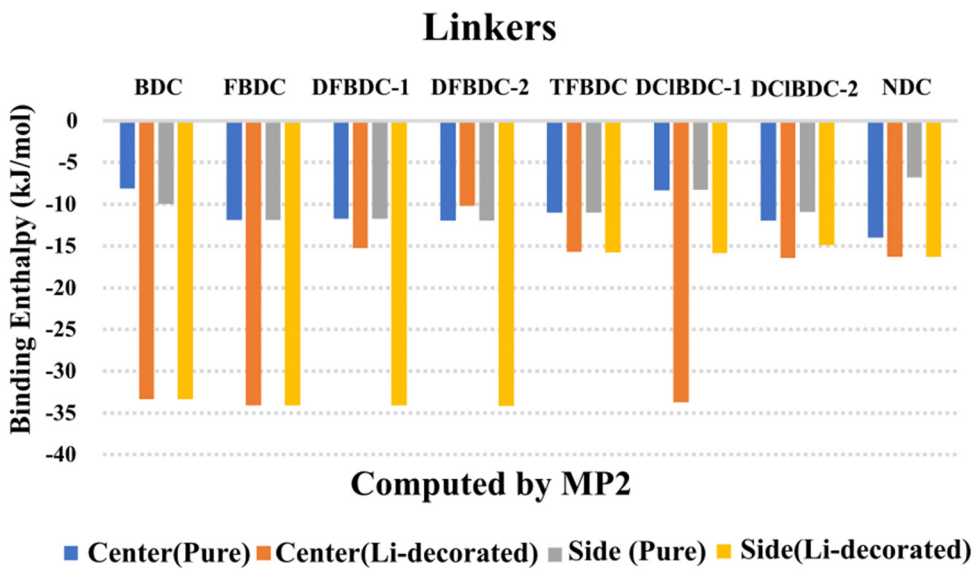


Fig. 6 The binding enthalpy ($\Delta H$) value of the adsorbed $CO_2$ molecule at the center and side positions of both the pure and Li-decorated linkers computed by the MP2 method.

functionalizing these linkers, the pore parameters (*i.e.*, pore size and shape, pore volume, and surface area) of the MOFs can be systematically modified to improve their selectivity and adsorption capacity towards a particular gas.[71] MOF-5 (or IRMOF-1) serves as a classic example of using isoreticular control to create various pore sizes through the judicious selection of organic linkers. Some highly porous MOFs for the adsorption of gases with their organic linkers, pore volume, and surface area are provided in Table 2.

### 4.2. Energy decomposition analysis (EDA)

EDA is one of the quantitative methods based on electronic structure calculations that tell about the contribution of various energy components/terms to the total interaction energy or binding enthalpy. It provides a better understanding of the factors involved in molecular interactions. The result of this analysis helps us to predict the properties of an interacting molecular system, which are difficult to analyze experimentally. In other words, the characteristics of the interaction between the linkers and $CO_2$ molecule are investigated by EDA, which provides crucial information for the design of novel MOFs with high adsorption capacity. Here, EDA has been performed for $CO_2$ adsorption at the side position of the BDC, FBDC, DFBDC-1, and DFBDC-2 linkers after obtaining the equilibrium structures. The contribution from different energy components to the total $\Delta H$ is shown in Fig. 7. Our study shows that the components of electrostatic, exchange, repulsion, polarization, and dispersion energies contribute to the total $\Delta H$ value for all the systems considered in the present investigation. Through this EDA, it is found that these complexes are effectively stabilized by electrostatic and polarization energy components and thus are the main contributing components to the total $\Delta H$. In other words, the study reveals that the interaction between the Li-decorated linkers and $CO_2$ molecule arises mainly from the electrostatic and polarization effects in terms of the energy components. The contribution from exclusion and dispersion energy components to the $\Delta H$ value was also found to be considerable. The repulsion energy term shows a positive contribution to the energy, which is obvious due to Pauli's exclusion principle. Thus, it is observed that among all the energy components, the electrostatic energy term is the most dominant one as depicted in Fig. 7.

Table 2 Some IRMOFs with their constituent linkers and pore parameters (Brunauer–Emmett–Teller (BET) and Langmuir surface areas and pore volume)

| MOFs | Linker | Surface area ($m^2\ g^{-1}$) | Pore volume ($cm^3\ g^{-1}$) | Ref. |
|---|---|---|---|---|
| IRMOF-1 | BDC | 2205 (BET) | 1.22 | 72 |
| IRMOF-3 | 2-$NH_2$-BDC | 1568 (BET) | 1.07 | 72 |
| IRMOF-6 | Cyclobutyl-BDC | 2516 (BET) | 1.14 | 73 and 74 |
| IRMOF-8 | 2,6-NDC | 1021 (BET) | 0.39 | 75 |
| MIL-101(Cr) | BDC | 5500 (Langmuir) | 1.9 | 76 |

### 4.3. Frontier molecular orbital (FMO)

To provide additional support to our calculated results and understand the interaction between the orbitals of adsorbed $CO_2$ and the organic linkers, we have extended our study to investigate the overlapping of molecular orbitals. The frontier molecular orbital analysis (FMO) was used to determine the energies of the highest occupied molecular orbital (HOMO) and lowest unoccupied molecular orbital (LUMO) levels. The HOMO and LUMO are collectively known as Frontier Molecular Orbitals (FMOs).[77] The difference in energies of the HOMO and LUMO gives an energy gap ($E_g$), which explains the stability as well as charge transfer taking place within the complex.[78] The high value of $E_g$ indicates the high kinetic stability and low chemical reactivity of the complex and hence it is chemically harder.[79,80] Since the physisorption process is a very weak

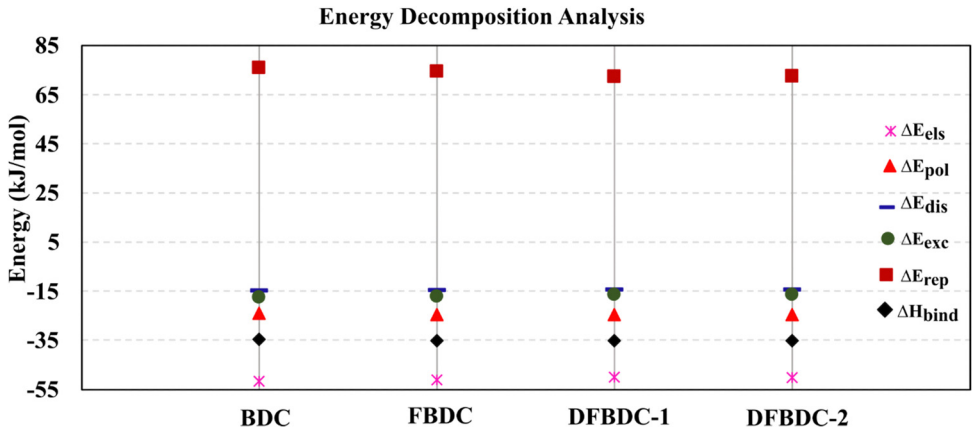


Fig. 7 The energy decomposition analysis (EDA) of $CO_2$ adsorption at the side position of the linkers. The electrostatic energy, polarization energy, dispersion energy, exchange energy, repulsion energy, and binding enthalpy are represented by $\Delta E_{els}$, $\Delta E_{pol}$, $\Delta E_{dis}$, $\Delta E_{exc}$, $\Delta E_{rep}$, and $\Delta H_{bind}$ respectively. They are expressed in kJ $mol^{-1}$.

interaction, to explain $CO_2$ physisorption on the Li–linker complexes, there is a need for the HOMO–LUMO energy gap and orbital interactions. The HOMO is associated with bonding orbitals (σ) with more electrons, and the LUMO is associated with anti-bonding orbitals (σ*) that do not have any electrons at the ground state.

This analysis was performed for all the linkers with adsorption of the $CO_2$ molecule at the side positions of the linkers. For both the pure and Li-decorated linkers, we investigated the $E_g$ value by calculating the energy difference between the HOMO and LUMO after $CO_2$ adsorption at the side position of the linkers. The computed energies of the HOMO and LUMO of all the linkers and the energy gap between them are provided in the ESI,† and the HOMO–LUMO energy gap is shown in Fig. 8. It is observed from Fig. 8 that there is a very small difference between the energy gap of FMOs in the pure and Li-decorated linkers; however, the energy gaps of the Li-decorated linkers are higher than those of the pure linkers, which proves that the complexes remained stable even after the Li-decoration. The contribution from the $CO_2$ molecule in the HOMO and LUMO calculations of the complexes alone is about −10.34 and 0.736 eV, respectively. The values of $E_g$ of the BDC, FBDC, DFBDC-1, and DFBDC-2 complexes are 5.33 eV, 5.09 eV, 4.83 eV, and 4.97 eV, respectively. Among all the complexes showing strong binding affinity, the highest HOMO–LUMO gap (5.33 eV) is observed for the BDC linker, where the energies of the HOMO and LUMO are −6.69 and −1.37 eV, respectively. The lowest value of the HOMO–LUMO gap is observed for the DFBDC-1 linker and the HOMO–LUMO energy gap is about 4.83 eV. The chances of electrons going from the HOMO to the LUMO decrease as the difference between the energies of FMOs increases. Hence these high values of the energy gap of the BDC, FBDC, DFBDC-1, and DFBDC-2 organic linkers demonstrate higher kinetic stability of the complexes.

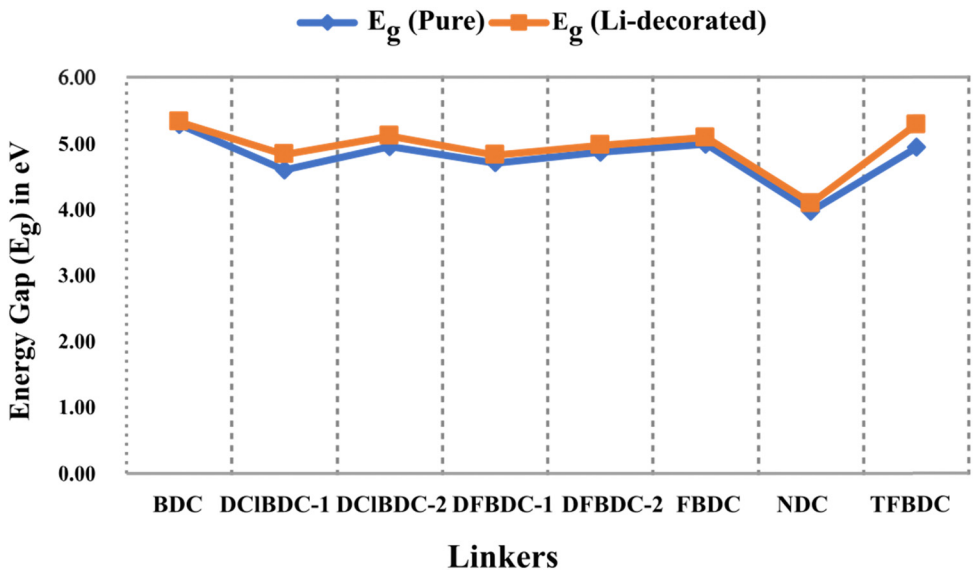


Fig. 8 The energy gap ($E_g$) between the HOMO and LUMO of both the pure and Li-decorated linkers. The energies are expressed in eV.

 

Next, Natural Bond Orbital (NBO) analysis was performed to observe the interaction between the orbitals of the $CO_2$ molecule, Li atoms, and the organic linkers. Fig. 9 shows the overlapping of the orbitals of both the pure and Li-decorated linkers with the adsorbed $CO_2$ molecule. Fig. 9(a)–(e) shows the orbital overlapping of pure linkers with the adsorbed $CO_2$ molecule, where interaction takes place between the p orbitals of C, O, and F atoms and the adsorbed $CO_2$ molecule. Similarly, Fig. 9(f)–(j) shows the overlapping of Li-decorated linkers, where the s orbitals of Li and p orbitals of C, O, and F atoms interact with the p orbital of the $CO_2$ molecule. The positive wave function, *i.e.*, the up spin of the electrons or alpha electrons is indicated by the red color orbital, while the negative wave function, *i.e.*, the down spin of the electrons or beta electrons is indicated by the blue color orbital. It is observed from Fig. 9 that the s orbital of Li and p orbitals of the C, O, and F atoms in the pure and Li-decorated linkers interact with the p orbital of the $CO_2$ molecule. These molecular interactions show that the $CO_2$ molecule is strongly adsorbed on the side position of the BDC, FBDC, DFBDC-1, and DFBDC-2 linkers. It is observed from Fig. 9 that for $CO_2$ adsorption at the side position of the NDC linker, a major part of the electron/charge density comes from the atoms constituting the pristine NDC linker.

Thus, it is clear from the above discussion that the kinetic stability of the complexes remained even after Li-decoration. The orbital overlapping of the $CO_2$ molecule and the BDC, FBDC, DFBDC-1, and DFBDC-2 linkers depicts a large $C_T$ value and is therefore responsible for the high binding enthalpy value. However, despite the large surface area, $CO_2$ adsorption on the Li-decorated NDC linker is low due to weak hybridization between the $CO_2$ molecule and the Li-atoms.

## 5. Conclusions

The search for more stable materials with durability, reusability, and cost efficiency is of great importance. However, the possibility of synthesizing highly porous MOFs using simple, cost-effective, and stable organic linkers remains a challenge. Organic bridging ligands or linkers are crucial for $CO_2$ adsorption on MOFs as they play a significant role in $CO_2$ capture. Functionalizing the organic ligands in MOFs is a well-known method to enhance the $CO_2$ adsorption capacity of MOFs. Here, we have computationally explored the impact of functionalizing the organic bridging linkers of the MOF materials with the different numbers of fluorine and chlorine atoms constituting the pure linkers and decorating these linkers with a light electropositive element (*i.e.*, Li) on the $CO_2$ adsorption capacity using molecular model systems. Both the B3LYP-D3 and MP2 methods with the cc-pVTZ basis set have been used to provide quantitative insight into the strength of $CO_2$ adsorption on the fluorinated and

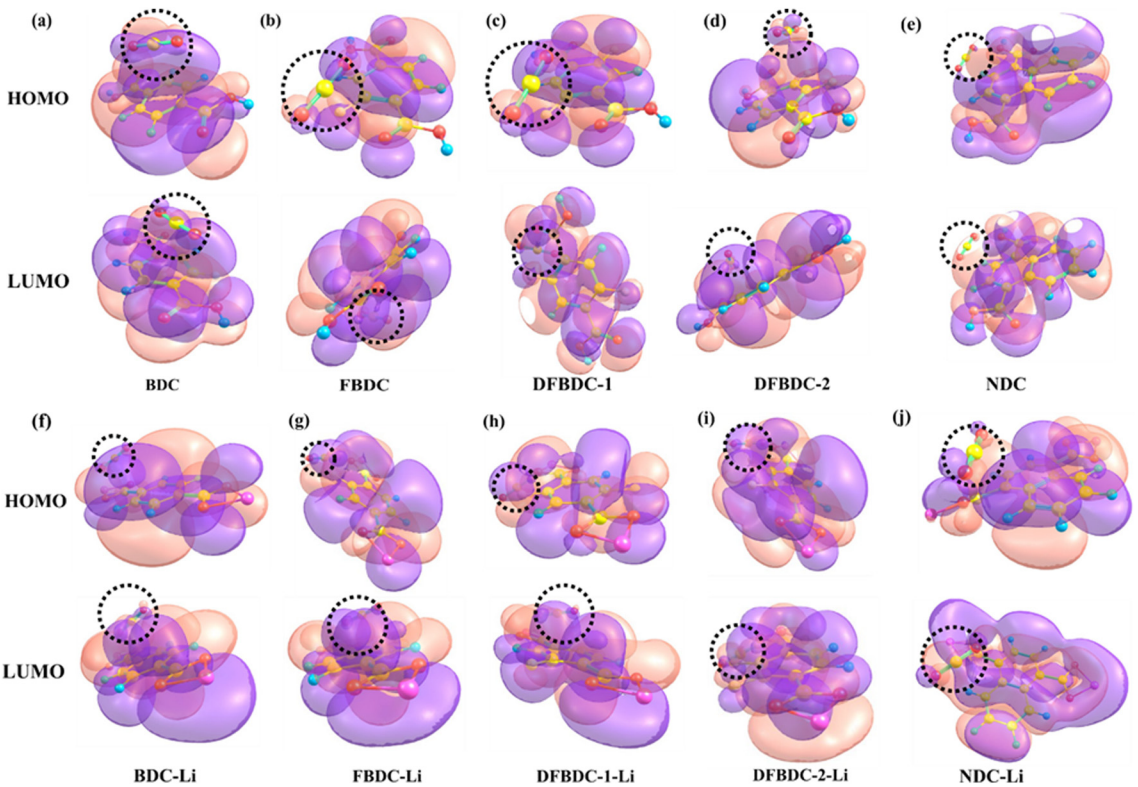


Fig. 9 The HOMO–LUMO projections of $CO_2$ adsorption at the side position of pure and Li-decorated linkers: (a) the BDC linker, (b) the FBDC linker, (c) the DFBDC-1 linker, (d) the DFBFC-2 linker, (e) the NDC linker, (f) the BDC-Li-decorated linker, (g) the FBDC–Li-decorated linker, (h) the DFBDC-1–Li-decorated linker, and (i) the DFBDC-2–Li-decorated linker, and (j) the NDC–Li-decorated linker.

chlorinated linkers at the atomistic level, and the interaction energies obtained by both the methods are in reasonable accord. The results of our investigation revealed that the $CO_2$ adsorption at the center and side positions of the FBDC, DFBDC-1, DFBDC-2, and TFBDC linkers, the side position of the DClBDC-2 linker, and the center position of the NDC linkers exhibits favorable physisorption behavior, while $CO_2$ adsorption at the center position of the Li-decorated BDC, FBDC, and DClBDC-1 linkers and the side position of the BDC, FBDC, DFBDC-1, and DFBDC-2 linkers reflects a strong physisorption behavior, indicating that Li decoration is an efficient approach for designing linkers with highly improved affinity. Furthermore, the results of EDA reveal that the contribution of both the electrostatic and polarization energy components to the $\Delta H$ is the most dominant one. The high energy gap ($E_g$) of the complexes revealed their kinetic stability even after Li-decoration.

The present study deals only with the organic linkers of the MOFs for $CO_2$ adsorption; however, using isolated organic linkers presents limitations such as reduced surface area, lack of structural integrity, absence of metal sites, reduced chemical functionalities, slower adsorption kinetics, and thermal and chemical stabilities. Moreover, the effect of the fluorinated and chlorinated linkers integrated into MOFs at different conditions must be studied and synthesized to implement fluorine and chlorine-based MOFs in $CO_2$ capture successfully. Thus, designing MOFs. Thus, designing MOFs known for their high chemical and thermal stability is urgently required for $CO_2$ capture in humid environments. MOFs owing to their high porosity exhibit much better performance in many applications but may find limitations in $CO_2$ capture due to high thermal, chemical, and stability requirements. A hydrophobic linker can modify the hydrophobic nature of frameworks for $CO_2$ capture, aiding in achieving the required goal. We expect that the linkers studied in this work will help MOF researchers to synthesize stable metal–organic frameworks toward $CO_2$ capture with enhanced hydrothermal stabilities and present an encouraging step towards developing novel $CO_2$ adsorbing materials.

## Author contributions

Dr Pakhira set up the whole idea of this current research work, and Dr Pakhira and Ms Kahkasha Parveen computationally studied the complexes and their molecular and thermodynamic properties. Quantum calculations and non-periodic molecular models were designed and performed by Dr Pakhira and Ms Kahkasha Parveen. The whole manuscript writing and preparation of figures and tables have been performed by Ms Kahkasha Parveen and Dr Pakhira.

## Data availability

All the data related to this work have been provided in the ESI.† We have used the Gaussian16 suite code, and we have developed our own GNUPLOT and python scripts to generate the figures. We have used GaussView6.0 and ChemCraft1.8 to create molecular structures with their figures. The equilibrium structures with the coordination of all the systems (organic bridging ligands or linkers) considered in the present investigation have been provided in the ESI† to reproduce our computed data.

## Conflicts of interest

The authors have no conflicts of interest.

## Acknowledgements

We thank the Council of Scientific & Industrial Research (CSIR), Government of India for providing the research funds under the scheme no. 22/0883/23/EMR-II. We recognize and thank the Science and Engineering Research Board, Department of Science and Technology (SERB-DST), Government of India, for their financial and technical assistance under Grant No. CRG/2021/000572. Ms Kahkasha Parveen thanks INSPIRE, DST, Govt. of India, for providing her doctoral Inspire fellowship under the scheme number IF200014. The authors are grateful to the Science and Engineering Research Board Department of Science and Technology (SERB-DST), Government of India, under Grant No. ECR/2018/000255 and CRG/2021/000572, for providing the financial support for this research work and computing research facilities with the codes. We acknowledge the financial support from the SERB-DST and Council of Scientific and Industrial Research (CSIR), Government of India. Professor Srimanta Pakhira is supported by the Indian Institute of Technology Indore, Ministry of Education (MoE), Government of India and Ms Kahkasha Parveen is supported by the INSPIRE, DST, Government of India.

## References

1 N. Von Der Assen, L. J. Müller, A. Steingrube, P. Voll and A. Bardow, *Environ. Sci. Technol.*, 2016, **50**, 1093–1101.
2 A. Demessence, D. M. D'Alessandro, M. L. Foo and J. R. Long, *J. Am. Chem. Soc.*, 2009, **131**, 8784–8786.
3 A. Goeppert, M. Czaun, J. P. Jones, G. K. Surya Prakash and G. A. Olah, *Chem. Soc. Rev.*, 2014, **43**, 7995–8048.
4 Y. J. Choi, J. H. Choi, K. M. Choi and J. K. Kang, *J. Mater. Chem.*, 2011, **21**, 1073–1078.
5 R. Thiruvenkatachari, S. Su, H. An and X. X. Yu, *Prog. Energy Combust. Sci.*, 2009, **35**, 438–455.
6 M. Wang, A. Lawal, P. Stephenson, J. Sidders and C. Ramshaw, *Chem. Eng. Res. Des.*, 2011, **89**, 1609–1624.
7 M. Pellerano, P. Pré, M. Kacem and A. Delebarre, *Energy Procedia*, 2009, **1**, 647–653.
8 M. Sai Bhargava Reddy, D. Ponnamma, K. K. Sadasivuni, B. Kumar and A. M. Abdullah, *RSC Adv.*, 2021, **11**, 12658–12681.
9 H. Furukawa and O. M. Yaghi, *J. Am. Chem. Soc.*, 2009, **131**, 8875–8883.
10 W. Fan, X. Zhang, Z. Kang, X. Liu and D. Sun, *Coord. Chem. Rev.*, 2021, **443**, 213968.

 

11 S. Ma and H. C. Zhou, *Chem. Commun.*, 2010, **46**, 44–53.
12 S. Cavenati, C. A. Grande and A. E. Rodrigues, *J. Chem. Eng. Data*, 2004, **49**, 1095–1101.
13 B. Wang, A. P. Côté, H. Furukawa, M. O'Keeffe and O. M. Yaghi, *Nature*, 2008, **453**, 207–211.
14 Z. Liang, M. Marshall and A. L. Chaffee, *Energy Fuels*, 2009, **23**, 2785–2789.
15 D. Land and E. D. Carlson, *Phys. Lett. B*, 1992, **292**, 107–112.
16 H. Furukawa, K. E. Cordova, M. O'Keeffe and O. M. Yaghi, *Science*, 2013, **341**, 1230444.
17 M. H. Yap, K. L. Fow and G. Z. Chen, *Green Energy Environ.*, 2017, **2**, 218–245.
18 M. Ding, X. Cai and H. L. Jiang, *Chem. Sci.*, 2019, **10**, 10209–10230.
19 P. D. C. Dietzel, V. Besikiotis and R. Blom, *J. Mater. Chem.*, 2009, **19**, 7362–7370.
20 K. S. Walton, A. R. Millward, D. Dubbeldam, H. Frost, J. J. Low, O. M. Yaghi and R. Q. Snurr, *J. Am. Chem. Soc.*, 2008, **130**, 406–407.
21 E. Klontzas, A. Mavrandonakis, G. E. Froudakis, Y. Carissan and W. Klopper, *J. Phys. Chem. C*, 2007, **111**, 13635–13640.
22 T. Düren, L. Sarkisov, O. M. Yaghi and R. Q. Snurr, *Langmuir*, 2004, **20**, 2683–2689.
23 Y. Liu, J. Liu, M. Chang and C. Zheng, *Fuel*, 2012, **95**, 521–527.
24 Z. Mai and D. Liu, *Cryst. Growth Des.*, 2019, **19**, 7439–7462.
25 Q. Yang, C. Zhong and J. F. Chen, *J. Phys. Chem. C*, 2008, **112**, 1562–1569.
26 A. Torrisi, C. Mellot-Draznieks and R. G. Bell, *J. Chem. Phys.*, 2009, **130**, 194703.
27 A. Torrisi, C. Mellot-Draznieks and R. G. Bell, *J. Chem. Phys.*, 2010, **132**, 044705.
28 S. Pakhira and J. L. Mendoza-Cortes, *J. Phys. Chem. C*, 2020, **124**, 6454–6460.
29 N. Sinha and S. Pakhira, *Mol. Syst. Des. Eng.*, 2022, **7**, 577–591.
30 A. Mavrandonakis, E. Klontzas, E. Tylianakis and G. E. Froudakis, *J. Am. Chem. Soc.*, 2009, **131**, 13410–13414.
31 A. Mavrandonakis, E. Tylianakis, A. K. Stubos and G. E. Froudakis, *J. Phys. Chem. C*, 2008, **112**, 7290–7294.
32 G. Lim, K. B. Lee and H. C. Ham, *J. Phys. Chem. C*, 2016, **120**, 8087–8095.
33 C. Gu, Y. Liu, W. Wang, J. Liu and J. Hu, *Front. Chem. Sci. Eng.*, 2021, **15**, 437–449.
34 S. S. Han and W. A. Goddard, *J. Am. Chem. Soc.*, 2007, **129**, 8422–8423.
35 Y. Liu, J. Liu, M. Chang and C. Zheng, *J. Phys. Chem. C*, 2012, **116**, 16985–16991.
36 P. Aprea, D. Caputo, N. Gargiulo, F. Iucolano and F. Pepe, *J. Chem. Eng. Data*, 2010, **55**, 3655–3661.
37 S. Biswas, D. E. P. Vanpoucke, T. Verstraelen, M. Vandichel, S. Couck, K. Leus, Y.-Y. Liu, M. Waroquier, V. V. Speybroeck, J. F. M. Denayer and P. V. D. Voort, *J. Phys. Chem. C*, 2013, **117**, 22784–22796.
38 B. Mohan, Virender, R. Kadiyan, S. Kumar, V. Gupta, B. Parshad, A. A. Solovev, A. J. L. Pombeiro, K. Kumar and P. K. Sharma, *Microporous Mesoporous Mater.*, 2024, **366**, 112932.
39 B. Mohan, A. Kamboj, Virender, K. Singh, Priyanka, G. Singh, A. J. L. Pombeiro and P. Ren, *Sep. Purif. Technol.*, 2023, **310**, 123175.
40 S. Kumar, B. Mohan, C. Fu, V. Gupta and P. Ren, *Coord. Chem. Rev.*, 2023, **476**, 214876.
41 T. Sagara, J. Ortony and E. Ganz, *J. Chem. Phys.*, 2005, **123**, 214707.
42 T. Sagara, J. Klassen, J. Ortony and E. Ganz, *J. Chem. Phys.*, 2005, **123**, 014701.
43 T. Sagara, J. Klassen and E. Ganz, *J. Chem. Phys.*, 2004, **121**, 12543–12547.
44 M. J. Frisch, G. W. Trucks, H. B. Schlegel, G. E. Scuseria, M. A. Robb, J. R. Cheeseman, G. Scalmani, V. Barone, G. A. Petersson, H. Nakatsuji, X. Li, M. Caricato, A. V. Marenich, J. Bloino, B. G. Janesko, R. Gomperts, B. Mennucci and J. B. Hratch, *Gaussian 16 (Revision C.01)*, Gaussian, Inc., Wallingford CT, 2016.
45 S. Grimme, *J. Comput. Chem.*, 2006, **27**, 1787–1799.
46 S. Grimme, J. Antony, S. Ehrlich and H. Krieg, *J. Chem. Phys.*, 2010, **132**, 154104.
47 J. Hui, N. B. Schorr, S. Pakhira, Z. Qu, J. L. Mendoza-Cortes and J. Rodríguez-López, *J. Am. Chem. Soc.*, 2018, **140**, 13599–13603.
48 S. Pakhira and J. L. Mendoza-Cortes, *Phys. Chem. Chem. Phys.*, 2019, **21**, 8785–8796.
49 S. Pakhira, K. P. Lucht and J. L. Mendoza-Cortes, *J. Chem. Phys.*, 2018, **148**, 064707.
50 Y. Lei, S. Pakhira, K. Fujisawa, X. Wang, O. O. Iyiola, N. Perea López, A. Laura Elías, L. Pulickal Rajukumar, C. Zhou, B. Kabius, N. Alem, M. Endo, R. Lv, J. L. Mendoza-Cortes and M. Terrones, *ACS Nano*, 2017, **11**, 5103–5112.
51 S. Pakhira and J. L. Mendoza-Cortes, *J. Phys. Chem. C*, 2018, **122**, 4768–4782.
52 X. B. Feng and N. M. Harrison, *Phys. Rev. B: Condens. Matter Mater. Phys.*, 2004, **69**, 132502.
53 M. F. Peintinger, D. V. Oliveira and T. Bredow, *J. Comput. Chem.*, 2013, **34**, 451–459.
54 Chemcraft, Graphical software for visualization of quantum chemistry computations, **https://www.chemcraftprog.com**.
55 R. Dennington, T. A. Keith and J. M. Millam, *GaussView, Version 6.1.*, Semichem Inc., Shawnee Mission KS, 2019.
56 P. Su and H. Li, *J. Chem. Phys.*, 2009, **131**, 014102.
57 M. W. Schmidt, K. K. Baldridge, J. A. Boatz, S. T. Elbert, M. S. Gordon, J. H. Jensen, S. Koseki, N. Matsunaga, K. A. Nguyen, S. Su, T. L. Windus, M. Dupuis and J. A. Montgomery, *J. Comput. Chem.*, 1993, **14**, 1347–1363.
58 B. Petrovic, M. Gorbounov and S. Masoudi Soltani, *Microporous Mesoporous Mater.*, 2021, **312**, 110751.
59 M. Ding, R. W. Flaig, H.-L. Jiang and O. M. Yaghi, *Chem. Soc. Rev.*, 2019, **48**, 2783–2828.
60 S. A. A. Razavi and A. Morsali, *Coord. Chem. Rev.*, 2019, **399**, 213023.
61 A. Shahtalebi, M. Mar, K. Guérin and S. K. Bhatia, *Carbon*, 2016, **96**, 565–577.
62 Z. Yang, S. Wang, Z. Zhang, W. Guo, K. Jie, M. I. Hashim, O. Miljanić, D. E. Jiang, I. Popovs and S. Dai, *J. Mater. Chem. A*, 2019, **7**, 17277–17282.

63 F. Safari, M. Moradinasab, M. Fathipour and H. Kosina, *Appl. Surf. Sci.*, 2019, **464**, 153–161.
64 A. Blomqvist, C. M. Araújo, P. Srepusharawoot and R. Ahuja, *Proc. Natl. Acad. Sci. U. S. A.*, 2007, **104**, 20173–20176.
65 K. L. Mulfort and J. T. Hupp, *J. Am. Chem. Soc.*, 2007, **129**, 9604–9605.
66 Y. J. Choi, J. W. Lee, J. H. Choi and J. K. Kang, *Appl. Phys. Lett.*, 2008, **92**, 15–18.
67 D. Cao, J. Lan, W. Wang and B. Smit, *Angew. Chem., Int. Ed.*, 2009, **48**, 4730–4733.
68 M. K. Rana, H. S. Koh, J. Hwang and D. J. Siegel, *J. Phys. Chem. C*, 2012, **116**, 16957–16968.
69 W. L. Queen, M. R. Hudson, E. D. Bloch, J. A. Mason, M. I. Gonzalez, J. S. Lee, D. Gygi, J. D. Howe, K. Lee, T. A. Darwish, M. James, V. K. Peterson, S. J. Teat, B. Smit, J. B. Neaton, J. R. Long and C. M. Brown, *Chem. Sci.*, 2014, **5**, 4569–4581.
70 D. Yu, A. O. Yazaydin, J. R. Lane, P. D. C. Dietzel and R. Q. Snurr, *Chem. Sci.*, 2013, **4**, 3544–3556.
71 Y. Zhao, H. Wu, T. J. Emge, Q. Gong, N. Nijem, Y. J. Chabal, L. Kong, D. C. Langreth, H. Liu, H. Zeng and J. Li, *Chem. Eur. J.*, 2011, **17**, 5101–5109.
72 D. Britt, D. Tranchemontagne and O. M. Yaghi, *Proc. Natl. Acad. Sci. U. S. A.*, 2008, **105**, 11623–11627.
73 J. L. C. Rowsell and O. M. Yaghi, *J. Am. Chem. Soc.*, 2006, **128**, 1304–1315.
74 A. R. Millward and O. M. Yaghi, *J. Am. Chem. Soc.*, 2005, **127**, 17998–17999.
75 Y. Li and R. T. Yang, *J. Am. Chem. Soc.*, 2006, **128**, 726–727.
76 M. Latroche, S. Surblé, C. Serre, C. Mellot-Draznieks, P. L. Llewellyn, J. H. Lee, J. S. Chang, S. H. Jhung and G. Férey, *Angew. Chem., Int. Ed.*, 2006, **45**, 8227–8231.
77 H. Gao and Z. Liu, *RSC Adv.*, 2017, **7**, 13082–13091.
78 R. Hussain, M. Saeed, M. Y. Mehboob, S. U. Khan, M. Usman Khan, M. Adnan, M. Ahmed, J. Iqbal and K. Ayub, *RSC Adv.*, 2020, **10**, 20595–20607.
79 J. Aihara, *J. Phys. Chem. A*, 1999, **103**, 7487–7495.
80 Y. Ruiz-Morales, *J. Phys. Chem. A*, 2002, **106**, 11283–11308.

 